A MICOS–TIM22 Association Promotes Carrier Import into Human Mitochondria

Sylvie Callegari[1,†], Tobias Müller[1,†], Christian Schulz[1], Christof Lenz[2,3], Daniel C. Jans[4,5], Mirjam Wissel[1], Felipe Opazo[6,7], Silvio O. Rizzoli[6,7], Stefan Jakobs[4,5], Henning Urlaub[2,3], Peter Rehling[1,8] and Markus Deckers[1]

*1 - **Department of Cellular Biochemistry,** University Medical Center Göttingen, Humboldtallee 23, 37073 Göttingen, Germany*
*2 - **Bioanalytical Mass Spectrometry Group,** Max Planck Institute for Biophysical Chemistry, Am Fassberg 11, 37077 Göttingen, Germany*
*3 - **Department of Clinical Chemistry,** Bioanalytics, University Medical Center Göttingen, Robert-Koch-Strasse 40, 37075 Göttingen, Germany*
*4 - **Department of NanoBiophotonics,** Mitochondrial Structure and Dynamics Group, Max Planck Institute for Biophysical Chemistry, Am Fassberg, 11 37077 Göttingen, Germany*
*5 - **Clinic for Neurology,** University Medical Center Göttingen, Robert-Koch-Strasse 40, 37075 Göttingen, Germany*
*6 - **Center for Biostructural Imaging of Neurodegeneration,** University Medical Center Göttingen, von-Siebold-Strasse 3a, 37075 Göttingen, Germany*
*7 - **Department of Neuro- and Sensory Physiology,** University Medical Center Göttingen, Humboldtallee 23, 37073 Göttingen, Germany*
*8 - **Max Planck Institute for Biophysical Chemistry,** Am Fassberg 11, 37077 Göttingen, Germany*

***Correspondence to Peter Rehling:** Department of Cellular Biochemistry, University Medical Center Göttingen, Humboldtallee 23, 37073 Göttingen, Germany. peter.rehling@medizin.uni-goettingen.de*
https://doi.org/10.1016/j.jmb.2019.05.015
Edited by M Yaniv

Abstract

Mitochondrial membrane proteins with internal targeting signals are inserted into the inner membrane by the carrier translocase (TIM22 complex). For this, precursors have to be initially directed from the TOM complex in the outer mitochondrial membrane across the intermembrane space toward the TIM22 complex. How these two translocation processes are topologically coordinated is still unresolved. Using proteomic approaches, we find that the human TIM22 complex associates with the mitochondrial contact site and cristae organizing system (MICOS) complex. This association does not appear to be conserved in yeast, whereby the yeast MICOS complex instead interacts with the presequence translocase. Using a yeast *mic10*Δ strain and a HEK293T MIC10 knockout cell line, we characterize the role of MICOS for protein import into the mitochondrial inner membrane and matrix. We find that a physiological cristae organization promotes efficient import via the presequence pathway in yeast, while in human mitochondria, the MICOS complex is dispensable for protein import along the presequence pathway. However, in human mitochondria, the MICOS complex is required for the efficient import of carrier proteins into the mitochondrial inner membrane. Our analyses suggest that in human mitochondria, positioning of the carrier translocase at the crista junction, and potentially in vicinity to the TOM complex, is required for efficient transport into the inner membrane.

Introduction

Mitochondria are bound by two selectively permeable membranes; the outer membrane shields mitochondria from the cytosol and is equipped for the regulation of mitochondrial dynamics and communication with other cellular components. The highly selective inner membrane is rich in protein complexes required for oxidative phosphorylation, protein translocation, metabolite transport and metabolic processes such as iron–sulfur cluster biogenesis [1–3]. To accommodate the many membrane-associated functions of mitochondria, the inner membrane folds to form protuberances called cristae. Protein complexes of differing function are asymmetrically and dynamically distributed along the tubular structure of

the cristae membrane, or along the flat inner boundary membrane, which runs parallel to the outer mitochondrial membrane [2,4,5].

Of the approximately 1000 nuclear-encoded proteins residing within yeast mitochondria, close to 700 are located within the inner membrane or the matrix [1,3]. Protein entry into these compartments involves intricate pathways that coordinate the translocase of the outer membrane (TOM complex) with the translocases of the inner membrane (TIM23 complex or TIM22 complex) [6]. The TIM23 complex, which specifically recognizes pre-sequence-containing proteins, is known to engage with the TOM complex during precursor translocation to form a transient supercomplex, thereby facilitating the handover of the precursor from the TOM complex to the TIM23 complex [7–11]. TIM23 substrates are then sorted into the inner membrane or translocated into the matrix. The TIM22 complex, also known as the carrier translocase, is instead specialized for the inner membrane insertion of hydrophobic, multi-transmembrane domain proteins that possess internal targeting signals [12–15]. Such substrates include the family of six-transmembrane spanning mitochondrial metabolite carriers, as well as four-transmembrane spanning components of the translocases, such as Tim23, Tim22 and Tim17 [16,17]. Carrier substrates are transported from the TOM complex to the TIM22 complex by the small TIM protein chaperone complex, which stabilizes the hydrophobic precursor on its journey through the aqueous IMS to the TIM22 complex [18–20].

It is currently unknown how carrier transport to the TIM22 complex is coordinated with the TOM complex, and this is further confounded by the fact that the architecture of the TIM22 complex is poorly conserved between yeast and human [15]. The TIM22 complex comprises a membrane-integrated module, which in yeast includes the pore-forming unit, Tim22, as well as Tim54, Tim18 and Sdh3 [21–24], and a peripheral membrane-associated module, consisting of Tim12, which is associated with Tim9/10 [18–20]. There have been no reports of direct contacts between the TOM complex and any of these components, although it was recently reported that Porin binds carrier precursors and recruits the TIM22 complex to promote carrier import [25]. This could mediate the handover of carrier precursors from the TOM complex to the TIM22 complex [25,26].

The structural components of the human TIM22 complex have only recently been elucidated. In addition to the conserved TIM22 pore-forming unit and the peripheral TIM10B unit (Tim12 in yeast), the human complex contains two metazoan specific components; TIM29 [27,28] and the acylglycerol kinase, AGK [29,30]. A particularly compelling feature of the human TIM22 complex is that it contacts TOM40 via TIM29 [28]. This indicates that a close spatial relationship between TIM22 and TOM could be important for precursor translocation in metazoa.

The mitochondrial contact site and cristae organizing system (MICOS) is a conserved multisubunit complex that stabilizes crista junctions. MICOS is composed of two subcomplexes; one comprising MIC10, MIC26, MIC27 and MIC13, and a second one consisting of MIC60, MIC19 and MIC25 [31–37]. The MICOS complex is central to the morphogenesis of the inner membrane. The MIC10-containing subcomplex stabilizes crista junctions and possesses membrane-bending characteristics, which shapes the crista junctions [38,39]. The MIC60-containing subcomplex is also capable of membrane shaping, but this complex extends across the intermembrane space and contacts components of the outer mitochondrial membrane, such as the TOM complex and the SAM complex [33,36,37,40–42]. The two MICOS subcomplexes are connected by the small integral membrane protein, MIC13, which is essential for integrity of the MIC10 subcomplex and for crista junction formation [32,43].

Given the interactions of MICOS with outer-membrane translocation complexes and its role in inner-membrane morphogenesis, it follows that MICOS may be required for the translocation of mitochondrial proteins. Indeed, in yeast, Mic60 was found to facilitate the import of substrates of the mitochondrial IMS assembly (MIA) by recruiting Mia40 to the intermembrane side of the TOM complex [33]. Furthermore, Mic60 promotes the insertion of β-barrel precursors into the outer mitochondrial membrane, possibly by supporting TOM–SAM supercomplex formation [42,44]. Curiously, an enrichment of MICOS complexes has also been observed following the isolation of inner and outer mitochondrial membrane contact sites containing an arrested, IMS spanning, GFP–Tim23 fusion protein [34]. In line with this observation, the TOM–TIM23 supercomplex, stabilized by an arrested precursor protein in yeast, has also been suggested to be in the vicinity of crista junctions [10]. However, it remains unclear whether MICOS has a role in the import of pre-sequence containing proteins via TIM23.

To date, the role of MICOS for protein translocation has mainly been explored in yeast. In this study, we endeavored to further investigate the mechanisms of human TIM22 function by identifying interaction partners of the metazoan specific component, TIM29. We uncovered an unexpected association with MICOS that is not conserved in yeast. Instead, in yeast, an interaction of the MICOS complex with the TIM23 complex was detected. Using a yeast *mic10*Δ strain and a HEK293T MIC10$^{-/-}$ cell line, we characterized the effect of MIC10 ablation on mitochondrial import via the TIM22 and TIM23 pathways in these two divergent eukaryotes and show that MICOS is important for the efficient inner membrane translocation of carrier proteins in human cells.

Results

The human carrier translocase associates with MICOS

We and others recently identified the TIM29 protein to be a core component of the TIM22 complex that is unique to metazoa [27,28]. To obtain a deeper insight into the proteome of the TIM22 complex and to identify specific interaction partners of TIM29, a stable HEK293T Flp-In cell line expressing an inducible C-terminal FLAG-tagged TIM29 construct was generated. Immunoisolation using FLAG antisera efficiently purified the ~400-kDa TIM22 complex (Fig. 1a). The complex was subsequently analyzed using Stable Isotope Labeling of Amino acids in Cell culture (SILAC)-based mass spectrometry to quantitatively determine complex constituents (Fig. 1b and Supplementary Table 1). All known TIM22 core components, TIM22, TIM29, AGK and TIM10B, were highly enriched, as were the accessory small TIMs (TIM9, TIM10A) and various mitochondrial carrier proteins, substrates of the TIM22 complex. Components of the TOM complex were also strongly enriched, consistent with previous findings showing that TIM29 contacts TOM40 [28].

Strikingly, several subunits of the MICOS complex were detected among the enriched proteins, namely, MIC60, MIC19, MIC25 and MIC27. The MIC60, MIC19 and MIC25 proteins make up the MICOS subcomplex, which preferentially interacts with components of the outer mitochondrial membrane, such as the TOM and SAM complexes [33,37,42,45]. Interestingly, both MIC60 and MIC19 were previously found to be enriched in proteomic analyses of AGK^{FLAG} and $TIM10B^{FLAG}$, and MIC60 alone was detected in mass spectrometry analysis of immunoisolated TIM22 [27–29]. To confirm the association between MICOS and the carrier translocase, immunoprecipitations of $TIM29^{FLAG}$, followed by SDS-PAGE and Western blotting, were performed. Both MIC19 and MIC60 co-immunoprecipitated with TIM29, as did MIC10 (Fig. 1c). Curiously, MIC10 was not detected in the mass spectrometric analysis, a phenomenon that is likely due to its hydrophobicity, which interferes with proteolytic digestion. In a reverse isolation of the MICOS complex, $MIC10^{FLAG}$ co-immunoprecipitated core components of the TIM22 complex (TIM29, TIM22 and AGK) (Fig. 1d). In summary, our analyses indicate an association between MICOS and the carrier translocase in human mitochondria.

To assess whether MICOS interacts with inner-membrane translocases *in vivo*, a proximity labeling approach was undertaken using the biotin conjugating system, BioID2 [46]. A construct was generated in which the HA-tagged biotin ligase, BioID2, was fused to the C-terminus of MIC10. Immunofluorescence microscopy of U2OS cells transfected with the construct verify mitochondrial localization (Fig. 2a). The $MIC10^{BioID2}$ construct was then expressed in HEK293T cells and immunoprecipitation with HA-antiserum confirmed that the fusion protein is efficiently incorporated into the MICOS complex (Fig. 2b). The proximity labeling reaction was carried out by supplementation of cells with biotin for 24 h. Biotinylated proteins were then precipitated using streptavidin beads, and isolated proteins were visualized by SDS-PAGE (Fig. 2c) and identified by mass spectrometry (Fig. 2d). Analysis of the BioID interactome revealed proteins enriched in the streptavidin pull down of the biotinylated $MIC10^{BioID2}$ samples (Supplementary Table 2). From the mitochondrial localized proteins, based on the Gene Ontology database (http://geneontology.org) [47] and on literature evidence, were several core MICOS components and known MICOS interaction partners, such as TOM70, SAM50 and OPA1 (Fig. 2d) [33,36,48]. Also present was TIM29, as well as several carrier proteins, further supporting the proximal location of MICOS to the TIM22 complex. Together, these data reveal a previously uncharacterized, but highly evident, association between the TIM22 complex and the MICOS complex in human mitochondria.

The yeast MICOS complex associates primarily with the presequence translocase

Much of the current knowledge of TIM22 function is based on studies carried out in the model yeast *Saccharomyces cerevisiae*. However, the architecture of the TIM22 complex in metazoa has diversified from that in yeast, and it could therefore be speculated that mammalian TIM22 function depends on a divergent protein interaction network. To determine whether the MICOS–TIM22 interaction is conserved in *S. cerevisiae*, the TIM22 complex was immunoisolated from a yeast strain expressing Tim18 with a C-terminal fusion with protein A [49]. In contrast to human cells, the MICOS components Mic60, Mic10 and Mic19 did not co-precipitate with the yeast TIM22 complex (Fig. 3a). To further support this finding, a yeast strain was generated in which the EPEA tag was genomically integrated downstream of the *MIC60* gene. The resulting $Mic60^{EPEA}$ fusion protein was isolated using an EPEA nanobody coupled to CNBr activated beads [50]. Although there was an efficient isolation of the MICOS complex, no co-purified TIM22 subunits could be detected (Fig. 3b). Instead, components of the TIM23 complex, Tim23 and Tim50, both co-precipitated with $Mic60^{EPEA}$. Likewise, immunoisolation of the TIM23 complex using Tim21 and Tim23 antisera co-purified Mic60 and Mic10, suggesting that in yeast the MICOS complex preferentially interacts with the TIM23 complex (Fig. 3c). Interestingly, the Mic60

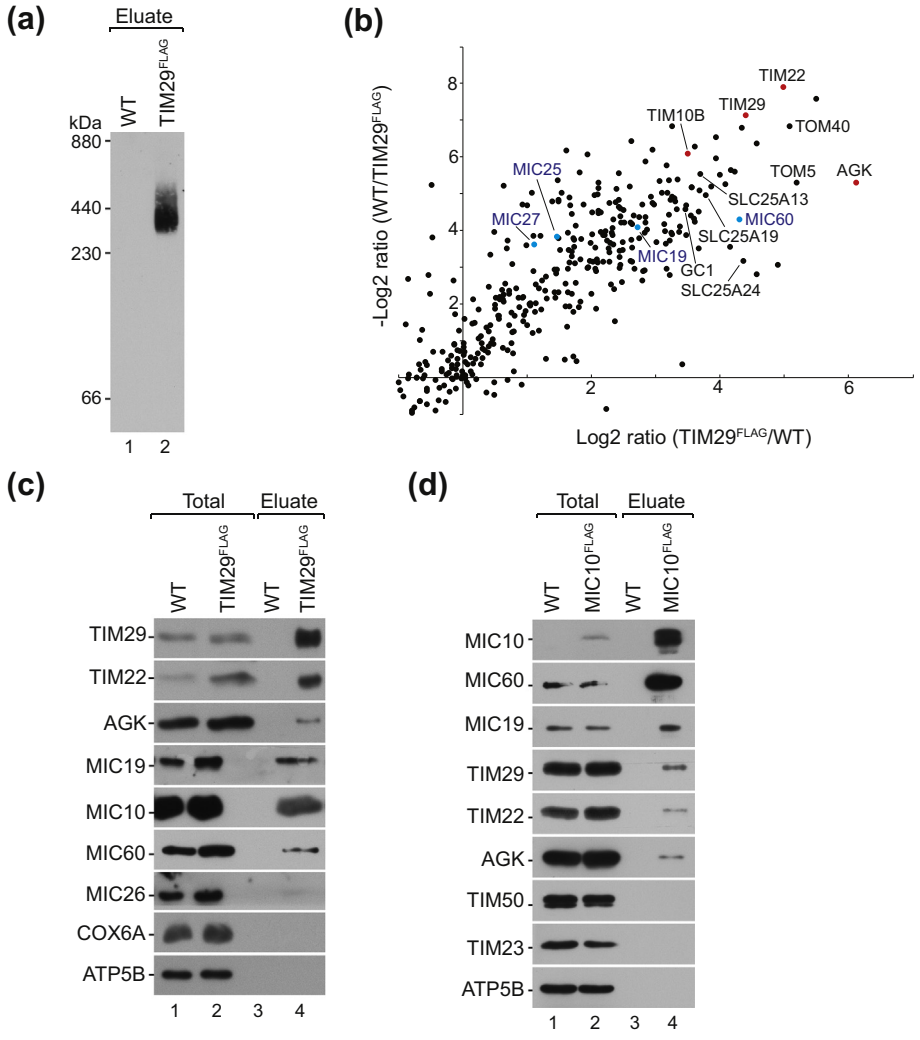

Fig. 1. The human TIM22 complex associates with MICOS. (a) BN-PAGE analysis of the TIM22 complex isolated via FLAG immunoisolation from purified HEK293T mitochondria, expressing TIM29^{FLAG}. (b) Quantitative mass spectrometry analysis of the TIM29^{FLAG} interactome. Control and TIM29^{FLAG} cells were differentially labeled using SILAC. Equal amounts of mitochondria were mixed, solubilized and subjected to anti-FLAG immunoprecipitation. Co-isolated proteins were analyzed by LC-MS. Two independent experiments were performed (with label switch). The normalized Log2 ratio is shown. Red, TIM22 complex components; blue, MICOS subunits. (c) TIM29^{FLAG} was immunoprecipitated from digitonin solubilized cells expressing TIM29^{FLAG} using FLAG anti-serum. Eluates were analyzed by SDS-PAGE, followed by Western blotting using antiserum for the indicated proteins. Total, 3%; eluate, 100% (except for MIC19, MIC10, MIC60, MIC26, COX6A and ATP5B, total 0.5%; eluate is 100%). (d) MIC10^{FLAG} was immunoprecipitated from digitonin solubilized MIC10^{FLAG} expressing HEK293T cells and analyzed as described in (c). Total, 3%; eluate, 100% (except for TIM29, TIM22, AGK, TIM50, TIM23 and ATP5B, total, 0.5%; eluate 100%).

interaction with Tim21 and Tim23 persisted in mitochondria from a *mic10*Δ yeast strain, which displays altered cristae organization [31] (Fig. 3c). This indicates that the MICOS–TIM23 association is independent of the Mic10 subcomplex and of the presence of physiological crista junctions.

This striking observation led us to test whether this MICOS–TIM23 interaction in yeast affects mitochondrial import. We measured the membrane potential of isolated mitochondria from wild-type and *mic10*Δ cells and observed no significant alterations of membrane potential (Fig. 4a). Therefore, to determine whether an intact MICOS complex is required for translocation across the inner membrane, *in vitro* import assays were performed using mitochondria from *mic10*Δ cells. Two radiolabeled presequence-containing proteins that are imported by the TIM23 complex were selected as model substrates; Atp2, a mitochondrial matrix targeted protein and Atp14, a sorted inner mitochondrial membrane protein. As a control, the ADP/ATP carrier, Aac1, was imported as a typical TIM22

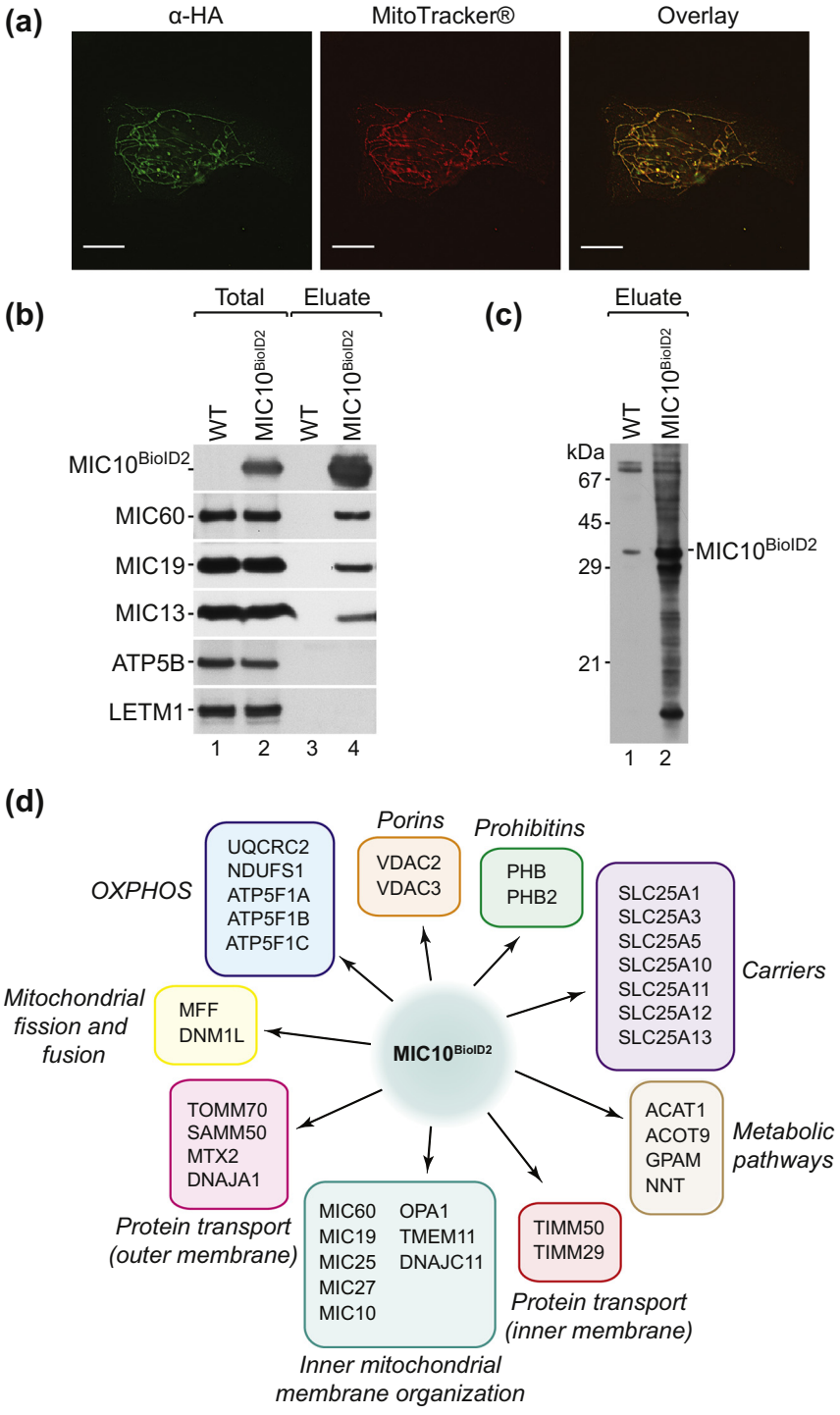

Fig. 2. Proximity biotinylation confirms TIM29 and MICOS interaction *in vivo*. (a) Immunofluorescence images of U2OS cells transiently transfected with MIC10^{BioID2}. HA antiserum was used to detect MIC10^{BioID2} and MitoTracker® orange CMTMRos was used to visualize mitochondria. The scale bar represents 15 μm. (b) Immunoprecipitation of MIC10^{BioID2} from whole-cell lysates using HA antiserum. Samples were anlayzed by SDS-PAGE, followed by Western blotting using the indicated antibodies. (c) Biotinylated proteins were isolated using streptavidin beads, eluted by incubation in Laemmli buffer for 5 min at 95 °C and analyzed by SDS-PAGE, followed by Western blotting. Biotinylated proteins were detected using anti-HRP (d) Selected mitochondrial proteins identified as enriched in mass spectrometry analysis of biotinylated proteins, isolated as described in panel C.

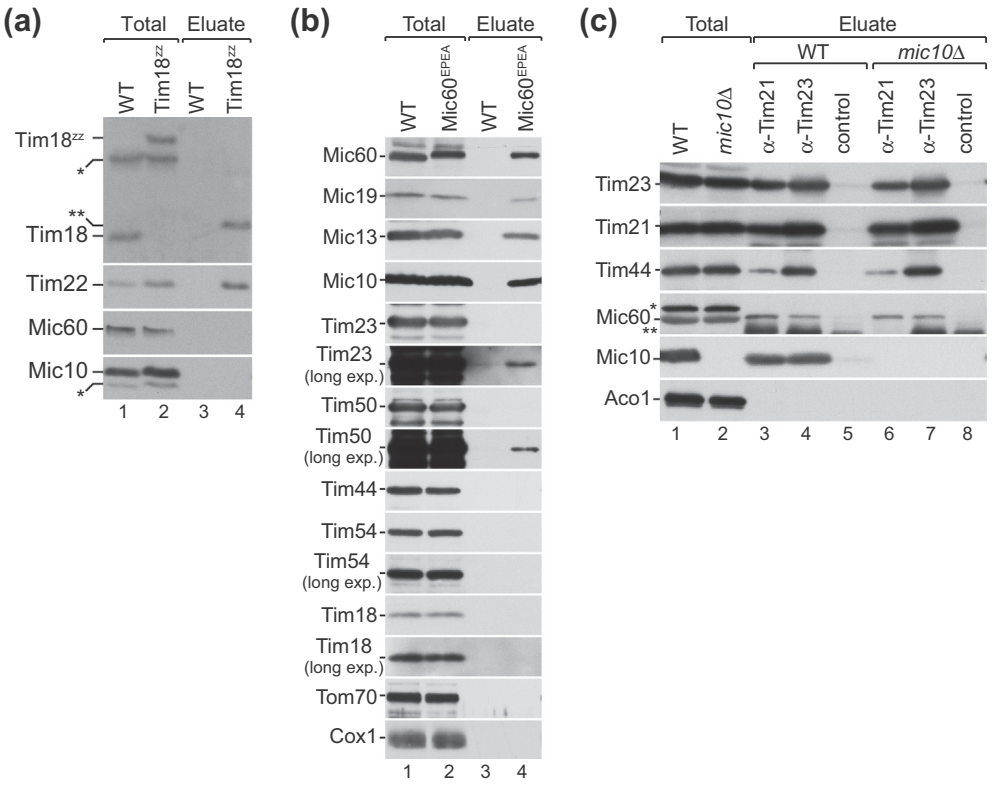

Fig. 3. Yeast MICOS associates with the presequence translocase. (a) The yeast TIM22 complex was purified from mitochondria isolated from an *S. cerevisiae* strain expressing Tim18^{zz} [49] and analyzed by SDS-PAGE, followed by Western blotting. Antibodies for Tim22 complex components and MICOS components were used to analyze co-isolated proteins. (b) Mitochondria were isolated from wild-type and Mic60^{EPEA} cells and after solubilization, Mic60^{EPEA} complexes were isolated using an EPEA-specific nanobody [50]. (c) The presequence translocase was immunoprecipitated using antisera against Tim23 or Tim21. Mitochondria from WT and *mic10*Δ yeast were solubilized and incubated with the indicated anti-sera. Immunoprecipitated complexes were analyzed by SDS-PAGE and Western blotting using the indicated antibodies.

substrate. Precursors were imported into wild-type and *mic10*Δ mutant mitochondria. Mitochondrial import of [^{35}S]Atp2 and [^{35}S]Atp14 was severely reduced, by more than 50%, in the absence of the MICOS complex (Fig. 4b), whereas assembly of the carrier Aac1 remained unaffected (Fig. 4c).

Ablation of Mic10 affects the formation of crista junctions, resulting in altered cristae morphology [31,33]. Altered cristae morphology is also observed upon loss of the ATPase dimerization factor Atp20, since dimerization induces membrane bending, which accounts for the high curvature regions of the cristae [52–54]. To determine whether the loss of cristae is responsible for the presequence pathway import defects in *mic10*Δ, *in vitro* import analyses were performed in mitochondria from a mutant strain lacking Atp20 [31,52]. In the *atp20*Δ mutant, import of [^{35}S]Atp2 and [^{35}S]Atp14 was affected to a similar extent as in *mic10*Δ mitochondria (Fig. 4d). As seen with mitochondria from *mic10*Δ, [^{35}S]Aac1 import via the carrier pathway was not reduced in mitochondria from the *atp20*Δ strain (Fig. 4e). Although these results clearly demonstrate the importance of cristae morphology for import of presequence-containing precursors, there does not appear to be a direct function of MICOS for translocation along this pathway. Based on these results, it is also evident that the MICOS–TIM22 interaction is specific to metazoa. Therefore, the function of this interaction was investigated further in human cells.

A MIC10 knockout cell line displays altered cristae morphology

In order to functionally investigate the relationship between MIC10 and the TIM22 complex, a HEK293T MIC10 knockout cell line (MIC10$^{-/-}$) was generated using the CRISPR/Cas9 system. The first exon was targeted and sequencing confirmation revealed the introduction of indels, resulting in a disruption of the open reading frame after the sixth amino acid and a subsequent premature stop codon (Fig. 5a). The absence of MIC10 expression was confirmed by Western

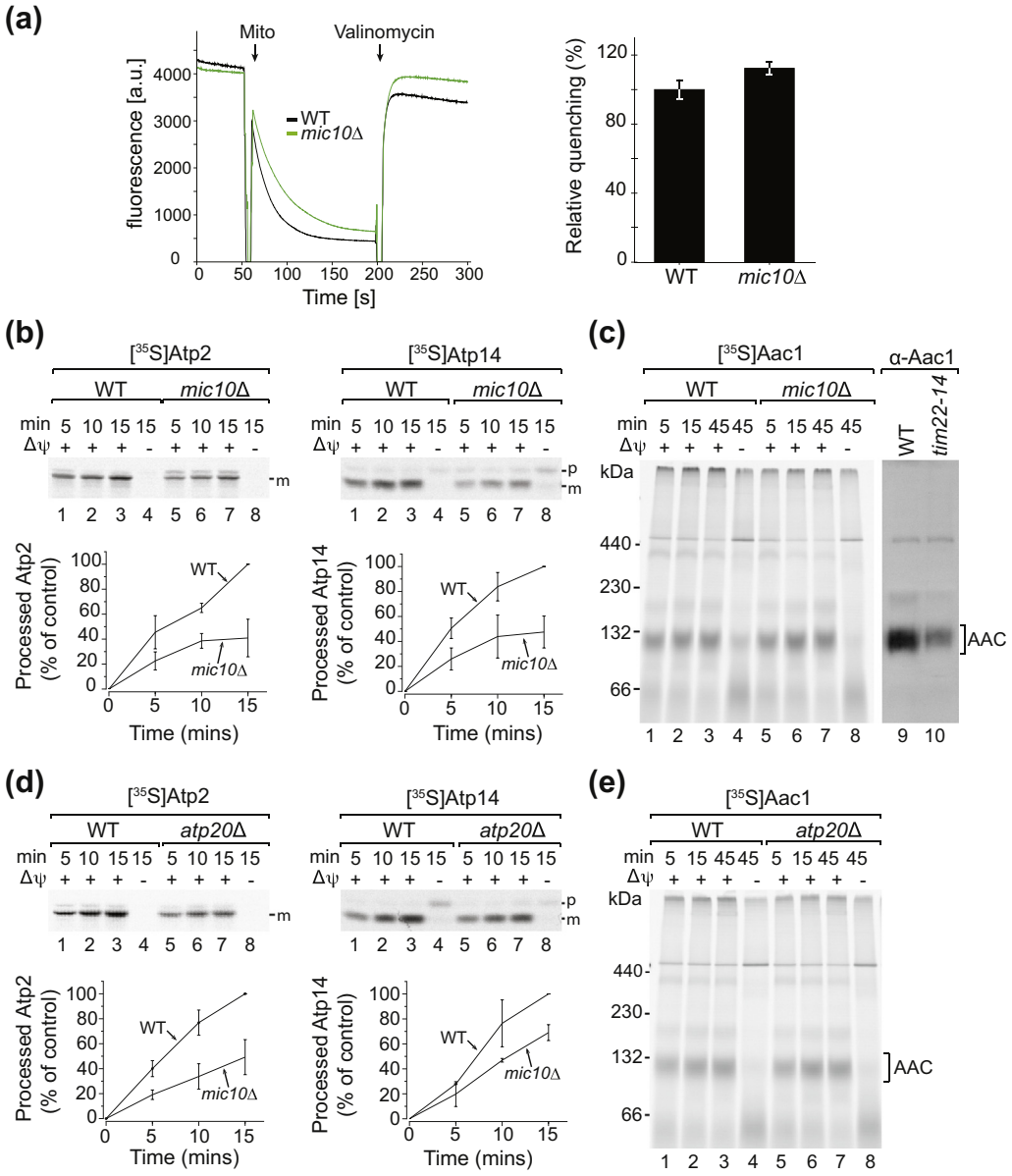

Fig. 4. MICOS is required for efficient import of TIM23 pathway substrates. (a) Mitochondrial membrane potential (Δψ) was measured in wild-type and *mic10*Δ yeast using the potential sensitive dye 3,3′-dipropylthiadicarocyanine iodide ($DiSC_3$) and monitoring of fluorescence. Relative fluorophore quenching, used to calculate Δψ, is shown in the adjacent bar graph (mean ± SEM, n = 3). (b) Radiolabeled Atp2 and Atp14 were imported into isolated mitochondria from wild-type and *mic10*Δ cells. Mitochondria were treated with proteinase K and samples analyzed by SDS-PAGE and digital autoradiography. Import of wild-type at the longest time point was set to 100% (mean ± SEM, n = 3). (c) Radiolabeled Aac1 was imported into isolated wild-type and *mic10*Δ mitochondria. Samples were solubilized, resolved by BN-PAGE and analyzed by digital autoradiography. A BN-PAGE analysis of the mature AAC complex in wild-type and *tim22–14* [51] using Aac1 antibody is shown alongside to show the running behavior of AAC at steady state. (d) Radiolabeled Atp2 and Atp14 were imported into isolated mitochondria from wild-type and *atp20*Δ and samples analyzed by SDS-PAGE and digital autoradiography. Import of wild-type at the longest time point was set to 100% (mean ± SEM, n = 3). Quantifications from three separate experiments are shown. (e) Radiolabeled Aac1 was imported into isolated wild-type and *mic10*Δ mitochondria. Samples were solubilized in digitonin, resolved by BN-PAGE analysis and analyzed by digital autoradiography. P, precursor; m, mature.

blotting. As described in yeast, disruption of MIC10 had no effect on the steady-state levels of MIC19 and MIC60, indicating that the MIC60 subcomplex is stable (Fig. 5b). However, MIC13 protein levels were almost completely abolished, suggesting dissociation of the MIC10 subcomplex. This was reversed upon expression of $MIC10^{FLAG}$ in $MIC10^{-/-}$ cells (Fig. 5b).

Complete ablation of MIC10 caused the typical altered cristae morphology seen in yeast *mic10*Δ [31] and in MEF cells that had undergone MIC10 shRNA-mediated knockdown [55]. This phenotype was complemented by the expression of $MIC10^{FLAG}$ in transfected $MIC10^{-/-}$ cells (Fig. 5b and c), supporting the essential role of MIC10 for cristae formation in human. Mitochondrial membrane potential in $MIC10^{-/-}$, assessed by uptake of tetramethylrhodamine-methylester (TMRM), remained unchanged and respirometry measurements did not reveal alterations in cellular oxygen consumption (Fig. 5d and e). Cell growth rate was also largely unaffected by the absence of MIC10 (Fig. 5f).

Interestingly, steady-state analyses revealed a reduction in mitochondrial carrier translocase constituents, notably TIM22 (levels at 72% ± 5.6%) (Fig. 5g). Likewise, TIM23 and TIM17B, components of the TIM23 complex, were also marginally affected. These translocase consitituents are all substrates of the TIM22 pathway. In addition, metabolite carrier substrates of TIM22 were also tested, specifically, the ADP/ATP carrier (ANT3) and the dicarboxylate carrier. ANT3 and dicarboxylate carrier levels were both decreased in $MIC10^{-/-}$ (Fig. 5g). In agreement with the steady-state analyses, BN-PAGE analyses showed a slight reduction in the 400 kDa TIM22 complex in $MIC10^{-/-}$ (Fig. 5h). In summary, lack of MIC10 affects the mitochondrial levels of tested carrier molecules, as well as translocase constituents that are transported along the carrier pathway.

MICOS promotes membrane integration of carrier proteins

To investigate whether MICOS is required for the import of proteins via the carrier pathway, *in vitro* import assays were carried out using mitochondria from wild-type and $MIC10^{-/-}$ cells. The radiolabeled precursors Su9-DHFR and COX4–1 were used as controls to analyze the transport of presequence-containing precursors to the matrix and inner membrane, respectively. The radiolabeled carrier ANT3 and the thiamine pyrophosphate carrier SLC25A19 were used as carrier pathway substrates. The import of both Su9-DHFR and COX4–1 was unaffected in mitochondria from $MIC10^{-/-}$, demonstrating that MIC10 is not required for import of presequence-containing precursors (Fig. 6a). Since mitochondria from $MIC10^{-/-}$ cells display a disrupted cristae morphology, these analyses show that in contrast to yeast, altered cristae morphology does not affect the presequence import pathway. However, the mitochondrial carrier pathway was drastically affected in $MIC10^{-/-}$ mitochondria. While ANT3 and SLC25A19 represent cargo molecules with different import kinetics, assembly efficiency of both ANT3 and SLC25A19 into the inner membrane was reduced by approximately 50% in $MIC10^{-/-}$ mitochondria (Fig. 6b).

Since steady-state levels of TIM22 are reduced in the absence of MIC10, we wanted to ascertain that the observed assembly defect is not a result of compromised TIM22 levels, but that MICOS has a more direct role in carrier import. To do this, an siRNA-mediated knockdown of TIM22 levels in wild-type cells was performed. The concentration of siRNA was titrated to a level in which only a mild knockdown of TIM22 (levels at 42% ± 8.7% compared to wild-type) was achieved in order to mimic the reduction of TIM22 protein levels observed in $MIC10^{-/-}$ cells (Fig. 6c). Mitochondria from $MIC10^{-/-}$ cells and from wild-type cells treated with TIM22 and control siRNA were isolated and used to assess the assembly of ANT3. Although ANT3 assembly was slightly affected in mitochondria with partial loss of TIM22, import into $MIC10^{-/-}$ mitochondria was drastically more affected (Fig. 6d). In fact, ANT3 assembly in mitochondria with slightly reduced TIM22 levels only appeared to be slowed, eventually reaching the same levels as in control cells at the 60-min time point. In contrast, ANT3 assembly in $MIC10^{-/-}$ mitochondria did not reach wild-type levels even after 60 min, signifying a greater degree of impairment than can be attributed to reduced TIM22 protein levels. Together, these data demonstrate that MICOS is required for the import of carrier proteins in human mitochondria.

Discussion

In this study, we uncover an association of the human carrier translocase with the MICOS complex. Using a $MIC10^{-/-}$ cell line, we show that this association is important for import of mitochondrial carrier proteins. Remarkably, the role of MICOS for the translocation of TIM22 substrates is not conserved in yeast. However, we find that a proper cristae architecture is essential for efficient translocation via the TIM23 complex in yeast. The TIM22 complex in human is the most evolutionary diverged of the translocases, having two metazoan specific components, AGK and TIM29. Along with the emergence of these components, it is likely that a restructuring of the interaction network of the TIM22 complex also occurred in higher eukaryotes. The finding that human TIM22 associates with MICOS, while the yeast MICOS preferentially interacts with the TIM23 complex exemplifies this concept.

The idea that TIM23 is positioned in the vicinity of crista junctions had previously emerged based on the observations that TIM–TOM supercomplexes appear enriched at crista junctions [10,34], but until now, an interaction between MICOS and TIM23 in yeast had not been detected. Here, we show that a small amount of TIM23 complex components co-precipitate with MICOS, supporting the idea that there is a propensity for the TIM23 complex to localize in the vicinity of

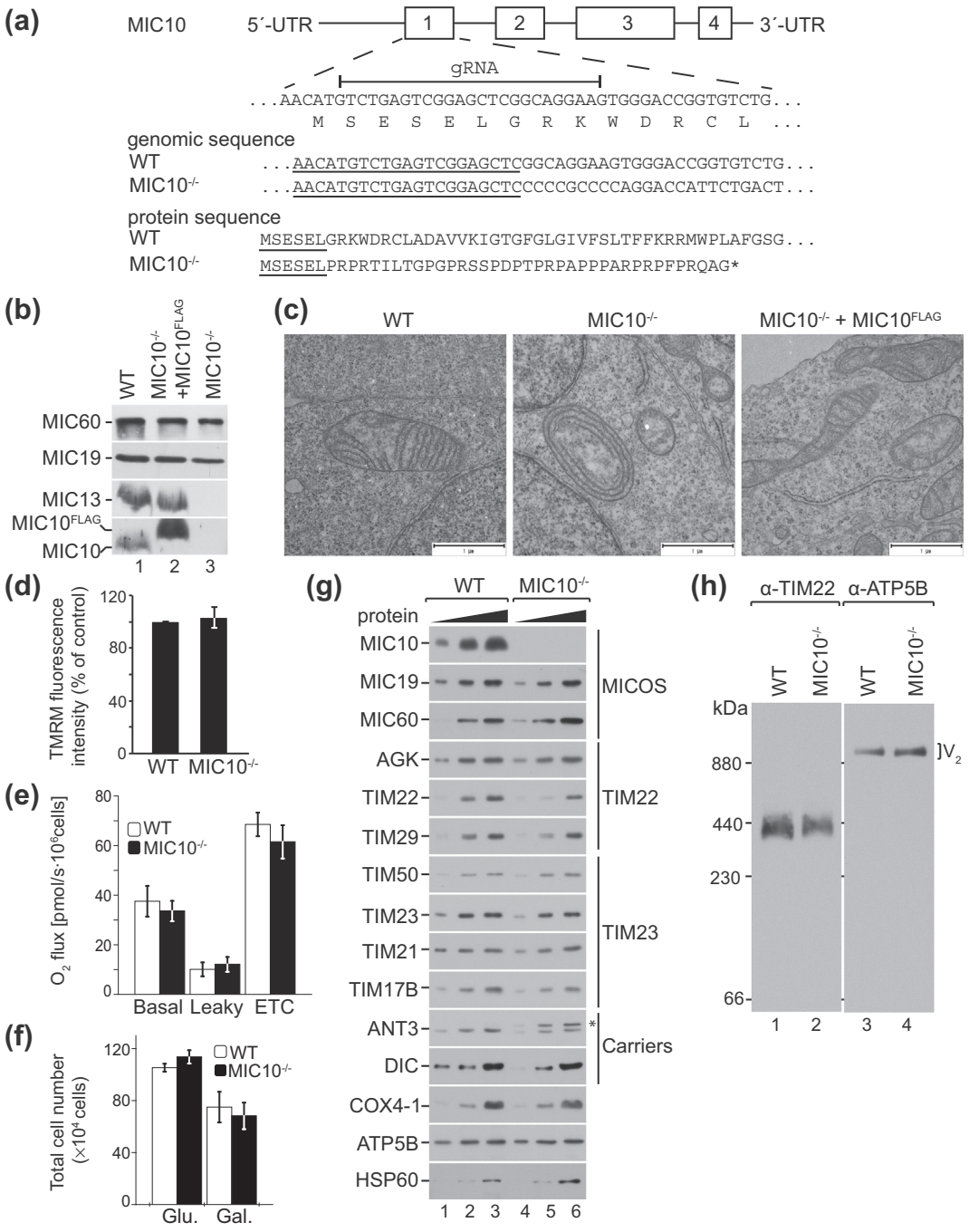

Fig. 5. MIC10 knockout disrupts cristae formation in HEK293T cells. (a) Graphic representation of MIC10 knockout strategy in HEK293T cells using CRISPR–Cas9. (b) Whole-cell lysates from the MIC10$^{-/-}$ cell line and from the MIC10$^{-/-}$ cell line rescued by transient transfection of MIC10^{FLAG} were analyzed by SDS-PAGE, followed by Western blotting. (c) Electron micrograph images of mitochondria from wild-type, MIC10$^{-/-}$ and MIC10$^{-/-}$ transiently transfected with MIC10^{FLAG}. The scale bar represents 1 μm. (d) Mitochondrial membrane potential in wild-type and MIC10$^{-/-}$ was measured by incubating cells with the potential sensitive probe TMRM, followed by flow cytometry. Quantification shown is the change in fluorescence intensity of MIC10$^{-/-}$, compared with wild-type (mean ± SEM, n = 3). (e) Relative oxygen consumption of WT and MIC10$^{-/-}$ cells was measured using the OROBOROS 2k system. Basal indicates basal metabolic rate. Leaky respiration was measured after complex V inhibition using oligomycin. The electron transfer capacity (ETC) was assessed after the addition of the uncoupling reagent CCCP. (mean ± SEM, n = 3). (f) Total cell numbers for wild-type and MIC10$^{-/-}$ were determined using a hemocytometer after 3 days of growth in DMEM supplemented with glucose or galactose (mean ± SEM, n = 3). (b) SDS-PAGE and Western blot analysis of mitochondria from wild-type and MIC10$^{-/-}$, using the indicated antibodies. (h) BN-PAGE and Western blot analysis of digitonin-solubilized mitochondria from wild-type and MIC10$^{-/-}$ using the indicated antibodies.

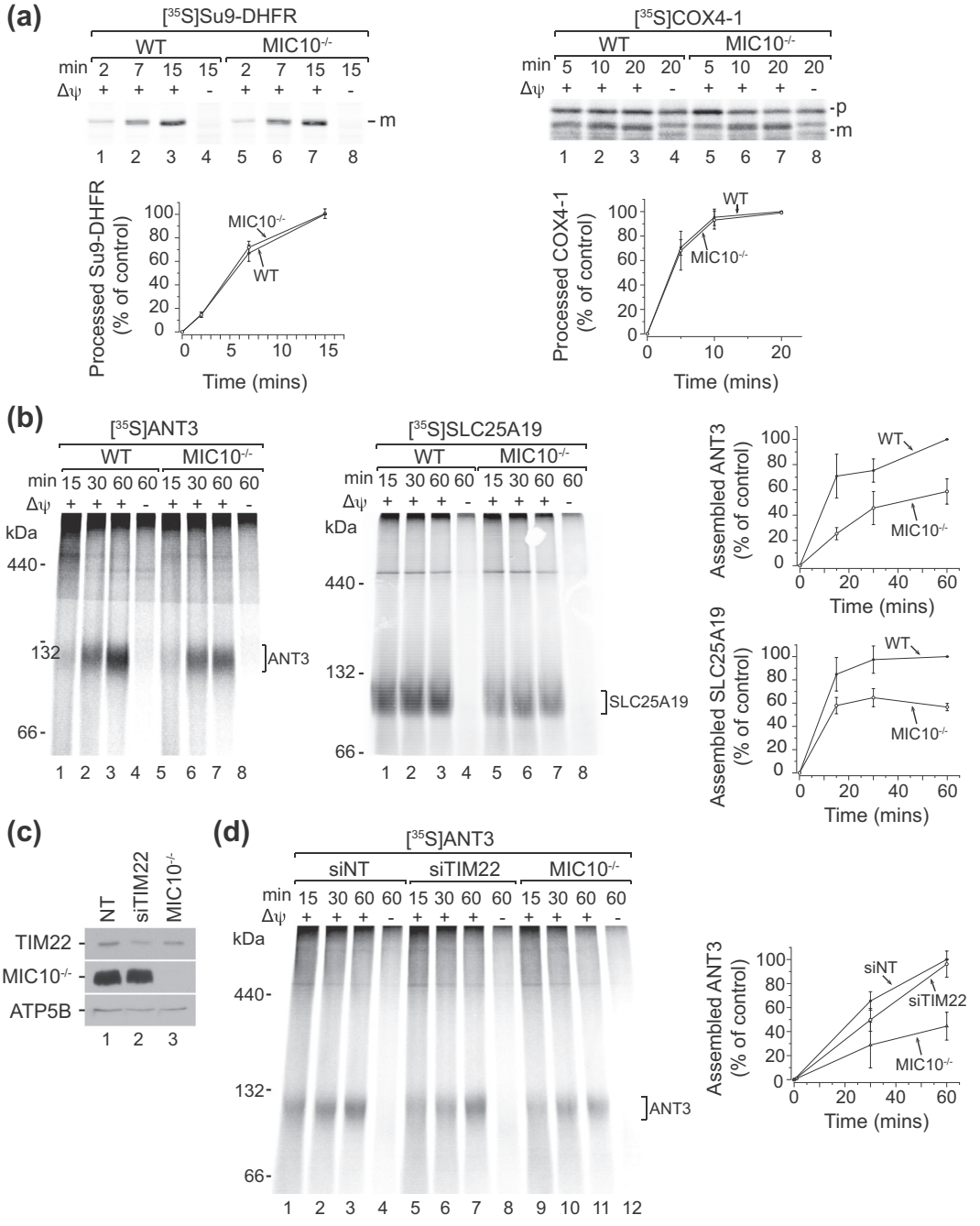

Fig. 6. Import along the carrier pathway is affected in MIC10$^{-/-}$. (a) Radiolabeled Su9-DHFR and COX4–1 were imported into isolated mitochondria from wild-type and MIC10$^{-/-}$ cells and analyzed by SDS-PAGE and digital autoradiography. Import of wild-type at the longest time point was set to 100% (mean ± SEM, n = 3). (b) Radiolabeled ANT3 and SLC25A19 were imported into isolated wild-type and MIC10$^{-/-}$ mitochondria. Samples were solubilized in digitonin buffer, resolved by BN-PAGE and analyzed by digital autoradiography. Import of wild-type at the longest time point was set to 100% (mean ± SEM, n = 3). (c) Mitochondria were isolated from HEK293T cells treated with TIM22 targeting siRNA (siTIM22), or non-targeting control siRNA (NT), and from MIC10$^{-/-}$. Mitochondria were analyzed by SDS-PAGE and Western blotting using the indicated antibodies. (d) Radiolabeled ANT3 was imported into isolated mitochondria from (c), solubilized in digitonin and analyzed by BN-PAGE and digital autoradiography. Import of siNT at the longest time point was set to 100% (mean ± SEM, n = 3).

MICOS. Interestingly, the TIM23–Mic60 association was maintained in the absence of Mic10 and thus in the absence of an intact MICOS complex. This finding indicates that the interaction is mediated by the Mic60 module. It has been shown that MICOS, via Mic60, forms larger complexes with the SAM and TOM complexes [33,36,42,56–58]. For these associations to occur, the inner and outer membrane must be in close contact. Hence, the positioning of TIM23 complexes by MICOS could facilitate precursor handover from the TOM complex to the TIM23 complex. Our import studies agree with the idea that the functional significance of the yeast TIM23–MICOS association is indeed linked to membrane morphology, as the presequence pathway import defect observed in *mic10*Δ yeast is recapitulated in *atp20*Δ mitochondria, which have a similar defect in cristae morphology.

In contrast to the presequence translocase, a juxtaposition of the outer and inner membranes is not thought to be essential for the transport of precursors via the TIM22 pathway in yeast. Here, precursor handover is facilitated by the soluble small TIM chaperones within the IMS [18,19]. This process may be less reliant on membrane morphology and may therefore explain why MICOS is not required for carrier import into yeast mitochondria. However, this scenario appears to be different in human cells where, although the small TIM chaperones are conserved, their function has not been deciphered and it is not known whether they assume the same roles as in yeast. In fact, it has been shown in human mitochondria that the small TIM complexes are more closely associated with the inner membrane and do not appear to be present as soluble complexes in the IMS [59]. Moreover, the human TIM22 complex has been found to directly contact the TOM40 pore via TIM29 [28]. These findings question the concept that small TIM hexamers shuttle precursors across the IMS to the TIM22 complex in human and instead proposes a mechanism by which precursor transfer from the TOM complex to the TIM22 complex occurs in a more direct and spatially confined manner. Our finding that the human TIM22 complex associates with MICOS supports this view and uncovers a mechanism that may assist with the positioning of TIM22 in close proximity to the TOM complex. Since there is no evidence that the TIM22 complex is primarily located at crista junction sites, it is likely that this association is dynamic and, at steady state, restricted to a subset of TIM22 complexes.

It has previously been reported that mammalian MICOS interacts with the TIM23 complex [45]; however, using the immunoprecipitation conditions in this study, TIM23 subunits were not detected. Nevertheless, upon solubilization and immunoprecipitation with a lower concentration of digitonin (0.05% instead of 1%), a weak detection of TIM23 and TIM21 protein in the MIC10^{FLAG} eluate could be observed, suggesting a more labile interaction of MICOS with TIM23 (data not shown). This is also supported by the presence of TIM50 in the proximity labeling analysis of MIC10^{BioID2}. Therefore, we cannot rule out that the TIM23 complex can still interact with MICOS in human cells, although it does not appear to have a functional role.

It is becoming increasingly clear that mitochondrial protein machines function in a dynamic and integrative manner [60]. A recent study by Ellenrieder *et al.* [25] discovered an unexpected cooperative action between Porin and TIM22 in yeast, which stimulates carrier import. The observation that Porin binds carrier precursors, while they are in complex with the small TIMs, and also interacts with the TIM22 complex, implies that Porin may act as a coupling factor in the TIM22 pathway [25]. Since Porin also associates with the TOM complex [26], it could be speculated that Porin mediates precursor handover from the TOM complex to TIM22. It remains to be determined whether this mechanism exists in human, but interestingly, all three isoforms of Porin in human, VDAC1, VDAC2 and VDAC3 were enriched in our TIM29^{FLAG} SILAC mass spectrometry analysis (Supplementary Table 1).

The finding that TIM22 and MICOS work synergistically in human mitochondria to drive the translocation of carrier proteins has important implications for understanding the mechanisms of TIM22 substrate translocation in human. Furthermore, this association links TIM22 activity to the regulation of MICOS, which is part of a larger network that encompasses proteins involved in metabolite handling, protein translocation, cell signaling, membrane architecture and mitochondrial dynamics [44]. Understanding these connections is especially relevant considering that reductions in TIM22 steady-state levels, as well as defective carrier import activity due to mutations in TIM22 components, have been linked to various pathologies [29,30,61,62].

Materials and Methods

Human cell culture

Human embryonic kidney cell lines (HEK293T-Flp-In™ T-Rex™) (ThermoFisher) were cultured in DMEM, supplemented with 10% (v/v) fetal bovine serum and incubated at 37 °C with 5% CO_2. For SILAC experiments, cells were grown for five passages on DMEM medium lacking arginine and lysine, supplemented with 10% (v/v) dialyzed fetal bovine serum, 600 mg/L proline, 42 mg/L arginine hydrochloride ($^{13}C_6$, $^{15}N_4$ arginine in "heavy" media) (Cambridge Isotope Laboratories) and 146 mg/L lysine hydrochloride ($^{13}C_6$, $^{15}N_2$ lysine in "heavy" media) (Cambridge Isotope Laboratories). For analysis of cell viability, 0.4% trypan blue (Gibco) was added to cells collected

in PBS. Afterward, cell numbers were measured directly with a hemocytometer. Mitochondrial isolations from HEK293T cells were performed as previously described [27].

Generation of cell lines

Constructs enabling inducible expression of C-terminally FLAG-tagged TIM29 and C-terminally FLAG-tagged MIC10 were generated by amplification of gene-specific fragments using HEK293T cDNA. Primers were designed based on the NCBI (National Center for Biotechnology Information) sequences: NM_138358.2 for TIM29 and NM_001032363.3 for MIC10. The FLAG peptide sequence was introduced prior to the stop codon in the reverse primer. Amplicons and pcDNA5/FRT/TO (Invitrogen) were digested with appropriate enzymes and ligated, and the final constructs were confirmed by sequencing. HEK293T cells were transfected with the constructs, together with the pOG44 vector (ThermoFisher) at approximately 50% confluency using GeneJuice® (Novagen) according to the manufacturer's instructions. Positive clones were selected using hygromycin B selection (Sigma-Aldrich, 100 µg/mL). Expression of the construct was induced using 1 µg/mL doxycycline (Sigma-Aldrich) 20 h prior to harvest. The MIC10^{BioID2} construct was generated by cloning PCR amplified MIC10 into a pcDNA 3.1 vector containing the BioID2 cassette (Addgene no. 74224) [46]. MIC10 was cloned N-terminal to the BioID2 cassette using the restriction enzymes NheI and BamHI.

The MIC10$^{-/-}$ HEK293T cell line was generated using CRISPR–Cas9 genome editing. Oligonucleotides were designed that encode a guide RNA targeting the first exon of MIC10. Oligonucleotides were then annealed and ligated into the pX330 vector. Cells were cotransfected with a GFP-encoding vector and single transfected cells were sorted into single wells of a 96-well plate. Clones were screened for the absence of MIC10 expression by immunoblotting. Disruption of the MIC10 gene was confirmed by genomic DNA extraction, PCR amplification of the region of disruption and subsequent sequencing. The siRNA-mediated knockdown of TIM22 was performed using 8 nM siRNA, as previously described [27]. For transient transfection of the MIC10^{BioID2} construct, cells that had been seeded 24 h prior were transfected using GeneJuice® (Novagen) according to the manufacturer's instructions.

Yeast strains and handling

S. cerevisiae yeast strains used in this study were derivatives of YPH499 [63]. The following yeast strains were used in this study: YPH499 (Mat a, ade2–101 his3-Δ200 leu2-Δ1 ura3–52 trp1-Δ63 lys2–801); Mic60^{EPEA} (Mat a, his3-Δ1 leu2Δ0 met15Δ0 ura3Δ0; *mic60*::*MIC60-EPEA-HIS3MX6*). Mic60^{EPEA} was generated using a modified pYM2 vector; briefly, the EPEA tag was introduced into pYM2 by site directed mutagenesis replacing the HA tag coding sequence. Tagging of Mic60 was achieved using pYM2-EPEA as previously described [64,65]. The Tim18^{zz} strain has previously been described [49], as has the *mic10*Δ strain [31]. Isolation of mitochondria from yeast cells was performed as previously described [66].

Affinity purifications

Isolated mitochondria were solubilized in buffer [20 mM Tris–HCl (pH 7.4), 100 mM NaCl, 0.5 mM EDTA, 10% (w/v) glycerol, 1 mM PMSF, 1% digitonin] at a final concentration of 1 mg/mL and incubated at 4 °C for 30 min. Lysates were cleared by centrifugation at 14,000*g* for 10 min at 4 °C and applied to affinity matrices. Anti-FLAG agarose affinity resin (Sigma-Aldrich) for FLAG immunoprecipitations and anti-HA agarose affinity resin (Sigma-Aldrich) for immuoprecipitations of MIC10^{BioID2} were used. For protein A and EPEA isolations, human-IgG Sepharose (MP Biomedicals) or purified EPEA nanobody, respectively, were coupled to CNBr-Activated Sepharose 4B (GE Healthcare) according to the manufacturer's protocol. Affinity columns for Tim21 and Tim23 immunoisolations were prepared by cross-linking protein A-Sepharose beads to Tim21 or Tim23 antisera. Protein lysates were incubated with affinity resins for 1 h at 4 °C on an end-over-end shaker. Unbound proteins were removed by centrifugation (100*g*, 1 min, 4 °C) through a minicolumn fitted with a filter. The beads were washed 10 times with W-buffer [25 mM Tris (pH 7.4), 150 mM NaCl, 1 mM EDTA, 10% (w/v) glycerol, 0.3% (w/v) digitonin, 1 mM PMSF]. Samples were eluted with 0.1 M glycine (pH 2.8), except in the case of EPEA isolation [W-buffer + 0.5 mg/mL EPEA peptide for 10 min at room temperature (RT)], protein A isolation [cleaved overnight at 4 °C with 0.4 mg/mL acetylated tobacco etch virus (Thermo Fisher Scientific) protease], or native elution of TIM29^{FLAG} [W-buffer + 5 µg/mL FLAG peptide (Sigma)].

BioID analysis

Cells transiently transfected cells with the MIC10^{BioID2} vector were supplemented with 50 µM biotin for 24 h. After washing with PBS, cells were harvested and frozen at −80 °C overnight. Cells were lysed by thawing on ice, resuspended in lysis buffer [50 mM Tris (pH 7.4), 150 mM NaCl, 0.1% SDS, 1% Triton X-100, 1 mM PMSF, 1× Complete Protease Cocktail (Roche)] and incubated for 5 min on ice. After centrifugation at 14,000*g* for 10 min, lysates were incubated with Streptavidin Beads (ThermoScientific)

overnight at 4 °C. Beads were washed 1× with washing buffer 1 [1% Na-deoxycholate, 1% Triton X-100, 500 mM NaCl, 1 mM EDTA, 50 mM Hepes (pH 7.5)], 2× with washing buffer 2 [200 mM LiCl, 0.5% NP-40, 0.5% Na-deoxycholate, 1 mM EDTA, 10 mM Tris (pH 8.1)], 3× with washing buffer 3 [50 mM NaCl, 50 mM Tris (pH 7.4)] and 2× with 10 mM ammonium bicarbonate. For elution, beads were incubated with Laemmli SDS buffer for 5 min at 95 °C.

Microscopy

For immunofluorescence microscopy, U2OS cells were grown on coverslips for at least 24 h. Cells were transfected with the $MIC10^{BioID2}$ construct as described above. At 24 h post-transfection, cells were incubated with MitoTracker® Orange CMTMRos (Life Technologies) for 15 min and then fixed with 4% formaldehyde for 20 min at 37 °C. Cells were washed in PBS and permeabilized with 0.2% Triton X-100 in PBS for 20 min at RT. Cells were washed again and the samples blocked with 1% BSA for 20 min at RT prior to incubation with mouse monoclonal anti-HA antibody for 1 h at RT. After washing in PBS, cells were incubated with the secondary antibody (Alexa Fluor 488 goat anti-mouse) for 30 min at RT. Samples were washed and finally embedded in histology mounting medium containing DAPI (Fluoroshield™). Images were recorded using a Delta Vision Spectris fluorescence microscope at 60× magnification, equipped with FITC (excitation 475/28, emission 523/36), TRITC (excitation 542/27, emission 594/45) and DAPI (excitation 390/18, emission 435/48) filter set. Image stacks were taken, images deconvoluted and a maximum projection of the stacks generated by merging the individual slices using the softWORx software (Applied Precision). For electron microscopy, cells were grown and imaged as previously described [67].

In vitro mitochondrial import

Radiolabeled precursor proteins were synthesized using rabbit reticulocyte lysate (Promega) in the presence of [^{35}S]methionine. Isolated mitochondria were diluted in import buffer for yeast [250 mM sucrose, 10 mM Mops/KOH (pH 7.2), 80 mM KCl, 2 mM KH_2PO_4, 5 mM $MgCl_2$, 5 mM methionine, 2 mM ATP, 2 mM NADH and 3% BSA], or for human [250 mM sucrose, 80 mM postassium acetate, 5 mM magnesium acetate, 5 mM methionine, 10 mM sodium succinate, 20 mM Hepes/KOH (pH 7.4) supplemented with 2 mM ATP, 1 mM dithiothreitol, 5 mM creatine phosphate and 0.1 mg/mL creatine kinase]. Import reactions were initiated by addition of 2% or 10% lysate for TIM23 substrates and TIM22 substrates, respectively. Samples were incubated with radiolabeled proteins for the indicated times. To stop the reaction, membrane potential was dissipated on ice using 8 mM antimycin A, 1 mM valinomycin and 10 mM oligomycin. Non-imported proteins were removed by proteinase K (20 µg/mL) treatment for 10 min on ice. PMSF (2 mM) was added to inactivate proteinase K for 10 min on ice. Mitochondria were collected, washed with SEM buffer [250 mM sucrose, 1 mM EDTA, 20 mM Mops (pH 7.2)] and used for SDS-PAGE analyses or BN-PAGE analyses. Results were visualized using digital autoradiography. Quantifications were performed using ImageQuant TL (GE Healthcare) using rolling ball background subtraction.

BN PAGE analyses

Mitochondria were solubilized in buffer [1% digitonin, 20 mM Tris/HCl (pH 7.4), 0.1 mM EDTA, 50 mM NaCl, 10% (w/v) glycerol and 1 mM PMSF] to a final concentration of 1 mg/mL for 30 min at 4 °C. Lysates were cleared by centrifugation at 14,000*g* for 10 min at 4 °C and 10× loading dye was added [5% Coomassie brilliant blue G-250, 500 mM 6-aminohexanoic acid, and 100 mM Bis-Tris (pH 7.0)]. Samples were loaded onto 6%–16% polyacrylamide gradient gels and separated as described [68].

Measurement of mitochondrial membrane potential

Mitochondrial membrane potential in human cells was assessed using the fluorescent dye TMRM. Cells were incubated for 30 min at 37 °C with staining solution (0.1 µM TMRM in DMEM) and subsequently washed, harvested and then fixed for 10 min in 2% PFA in PBS. Cells were then measured in PBS supplemented with 10% FBS, using a BD-Canto flow cytometer (Becton Dickinson), with excitation at 488 nm and detection with a 570 ± 10-nm emission filter.

Mitochondrial membrane potential in yeast was measured using a potential-sensitive dye 3,3′-dipropylthiadicarocyanine iodide ($DiSC_3(5)$). Mitochondria were diluted in a buffer containing 600 mM sorbitol, 1% (wt/vol) BSA, 10 mM $MgCl_2$ and 20 mM KPi (pH 7.4) to a concentration of 166 µg/mL. Changes in fluorescence were assessed with an F-7000 fluorescence spectrophotometer (Hitachi, JP), at RT, with excitation of 622 nm, emission at 670 nm and slits of 5 nm. After reaching a stable signal, components were added to the cuvette in the following order: 500 µL of buffer, $DiSC_3(5)$, 83 µg of mitochondria and 1 µM valinomycin (to compare relative differences in membrane potential, the difference in fluorescence before and after addition of valinomycin was used).

Sample preparation for mass spectrometry

Samples were reconstituted in 1× NuPAGE LDS Sample Buffer (Invitrogen) and separated on 4%–12% NuPAGE Novex Bis-Tris Minigels (Invitrogen). Gels were stained with Coomassie Blue for visualization purposes, and each lane sliced into 23 equidistant slices. After washing, gel slices were reduced with dithiothreitol, alkylated with 2-iodoacetamide and digested with Endopeptidase Trypsin (sequencing grade, Promega) overnight. The resulting peptide mixtures were then extracted, dried in a SpeedVac, reconstituted in 2% acetonitrile/0.1% formic acid (v/v) and prepared for nanoLC–MS/MS as described previously [69].

Oxygen consumption measurements

Oxygen consumption of whole cells was assessed using high-resolution respirometry (Oxygraph-2 k; Oroboros Instruments, Innsbruck, Austria) in 2 mL of DMEM, containing glucose at 37 °C. After assessing basal respiration, oligomycin (1.5 μM) was used to block the proton channel of Complex V to assess leaky respiration. Electron transport capacity was assessed following successive addition of carbonyl-cyanide-*m*-chlorphenylhydrazone (CCCP).

nanoLC–MS/MS analysis

Samples were enriched on a self-packed reversed phase-C18 precolumn (0.15 mm ID × 20 mm, Reprosil-Pur120 C18-AQ 5 μm, Dr. Maisch, Ammerbuch-Entringen, Germany) and separated on an analytical reversed phase-C18 column (0.075 mm ID × 200 mm, Reprosil-Pur 120 C18-AQ, 3 μm, Dr. Maisch) using a 30-min linear gradient of 5%–35% acetonitrile/0.1% formic acid (v/v) at 300 nL min^{-1}). The eluent was analyzed on a Q Exactive hybrid quadrupole/orbitrap mass spectrometer (ThermoFisher Scientific, Dreieich, Germany) equipped with a FlexIon nanoSpray source and operated under Excalibur 2.5 software using a data-dependent acquisition method. Each experimental cycle was of the following form: one full MS scan across the 350–1600 *m*/*z* range was acquired at a resolution setting of 70,000 FWHM, and AGC target of 1 * 10e6 and a maximum fill time of 60 ms. Up to the 12 most abundant peptide precursors of charge states 2 to 5 above a 2 * 10e4 intensity threshold were then sequentially isolated at 2.0 FWHM isolation width, fragmented with nitrogen at a normalized collision energy setting of 25%, and the resulting product ion spectra recorded at a resolution setting of 17,500 FWHM, and AGC target of 2 * 10e5 and a maximum fill time of 60 ms. Selected precursor *m*/*z* values were then excluded for the following 15 s. Two technical replicates per sample were acquired.

Data processing—SILAC-MS

Raw data were processed using MaxQuant Software version 1.5.2.8 (Max Planck Institute for Biochemistry, Martinsried, Germany). Proteins were identified against the UniProt Human Reference Proteome (v2017.02) along with a set of common laboratory contaminants. The search was performed with trypsine as enzyme and iodoacetamide as cysteine blocking agent. Up to two missed tryptic cleavages and methionine oxidation as a variable modification were allowed for. Instrument type "Orbitrap" was selected to adjust for MS acquisition specifics. FDR was adjusted to 1% on both peptide and protein levels. The arginine R10 and lysine K8 labels including the "Re-quantify" option were specified for relative protein quantitation. Perseus Software version 1.5.0.15 (Max Planck Institute for Biochemistry, Martinsried, Germany) was used to obtain relative protein quantitation values from the MaxQuant Software results and perform statistical evaluation.

Data processing—spectral counting

Peaklists were extracted from the raw data using Raw2MSMS software v1.17 (Max Planck Institute for Biochemistry, Martinsried, Germany). Protein identification was achieved using MASCOT 2.5.1 software (Matrixscience, London, United Kingdom) against the UniProtKB Human Reference Proteome (v2018.09) along with a set of common laboratory contaminants. The search was performed with trypsin as enzyme and iodoacetamide as cysteine blocking agent. Up to two missed tryptic cleavages and methionine oxidation as a variable modification were allowed for. Search tolerances were set to 10 ppm for the precursor mass and 0.05 Da for fragment masses, and ESI-QUAD-TOF specified as the instrument type.

Scaffold software version 4.8.6 (Proteome Software Inc., Portland, OR) was used to validate MS/MS-based peptide and protein identifications. FDR was adjusted to 1% on both peptide and protein levels. Proteins sharing significant peptide evidence were grouped into clusters. Relative quantification of proteins in the samples was achieved by analysis of variance of normalized spectral counts using a Benjamini–Hochberg multiple testing correction.

Supplementary data to this article can be found online at https://doi.org/10.1016/j.jmb.2019.05.015.

Acknowledgments

We are grateful to Dr. Abhishek Aich and Dr. Luis Daniel Cruz Zaragoza for their support. This work

was supported by the Deutsche Forschungsgemeinschaft (SFB1190; Projects P13, P.R.; P01, S.J.; P09, S.R. and Z02, H.U.) and the Max Planck Society (S.J., H.U. and P.R.).

Declaration of Competing Interest: Dr. Christian Schulz is now an employee of Elsevier BV without access or influence over the editorial process. The work presented here was prepared during his employment at the University Medical Center Göttingen, prior to his current employment with Elsevier.

Received 12 March 2019;
Received in revised form 10 May 2019;
Available online 17 May 2019

Keywords:
mitochondria;
MICOS;
TIM22;
TIM23;
mitochondrial carrier proteins

†S.C. and T.M. contributed equally to this work.

Abbreviations used:
MICOS, mitochondrial contact site and cristae organizing system; SILAC, Stable Isotope Labeling of Amino acids in Cell culture; RT, room temperature; TMRM, tetramethylrhodamine-methylester.

References

[1] F.-N. Vögtle, J.M. Burkhart, H. Gonczarowska-Jorge, C. Kücükköse, A.A. Taskin, D. Kopczynski, R. Ahrends, D. Mossmann, A. Sickmann, R.P. Zahedi, et al., Landscape of submitochondrial protein distribution, Nat. Commun. 8 (2017) 290.

[2] F. Vogel, C. Bornhövd, W. Neupert, A.S. Reichert, Dynamic subcompartmentalization of the mitochondrial inner membrane, J. Cell Biol. 175 (2006) 237–247.

[3] M. Morgenstern, S.B. Stiller, P. Lübbert, C.D. Peikert, S. Dannenmaier, F. Drepper, U. Weill, P. Höß, R. Feuerstein, M. Gebert, et al., Definition of a high-confidence mitochondrial proteome at quantitative scale, Cell Rep. 19 (2017) 2836–2852.

[4] C.A. Wurm, S. Jakobs, Differential protein distributions define two sub-compartments of the mitochondrial inner membrane in yeast, FEBS Lett. 580 (2006) 5628–5634.

[5] S. Stoldt, D. Wenzel, K. Kehrein, D. Riedel, M. Ott, S. Jakobs, Spatial orchestration of mitochondrial translation and OXPHOS complex assembly, Nat. Cell Biol. 20 (2018) 528–534.

[6] J. Dudek, P. Rehling, M. van der Laan, Mitochondrial protein import: common principles and physiological networks, Biochim. Biophys. Acta 1833 (2013) 274–285.

[7] M. Schleyer, W. Neupert, Transport of proteins into mitochondria: translocational intermediates spanning contact sites between outer and inner membranes, Cell 43 (1985) 339–350.

[8] C. Schulz, A. Schendzielorz, P. Rehling, Unlocking the presequence import pathway, Trends Cell Biol. 25 (2015) 265–275.

[9] M. Horst, S. Hilfiker-Rothenfluh, W. Oppliger, G. Schatz, Dynamic interaction of the protein translocation systems in the inner and outer membranes of yeast mitochondria, EMBO J. 14 (1995) 2293–2297.

[10] V.A.M. Gold, R. Ieva, A. Walter, N. Pfanner, M. van der Laan, W. Kühlbrandt, Visualizing active membrane protein complexes by electron cryotomography, Nat. Commun. 5 (2014) 4129.

[11] A. Chacinska, P. Rehling, B. Guiard, A.E. Frazier, A. Schulze-Specking, N. Pfanner, W. Voos, C. Meisinger, Mitochondrial translocation contact sites: separation of dynamic and stabilizing elements in formation of a TOM–TIM–preprotein supercomplex, EMBO J. 22 (2003) 5370–5381.

[12] N. Pfanner, W. Neupert, Distinct steps in the import of ADP/ATP carrier into mitochondria, J. Biol. Chem. 262 (1987) 7528–7536.

[13] K. Brandner, P. Rehling, K.N. Truscott, The carboxyl-terminal third of the dicarboxylate carrier is crucial for productive association with the inner membrane twin-pore translocase, J. Biol. Chem. 280 (2005) 6215–6221.

[14] P. Rehling, K. Brandner, N. Pfanner, Mitochondrial import and the twin-pore translocase, Nat. Rev. Mol. Cell Biol. 5 (2004) 519–530.

[15] Y. Kang, L.F. Fielden, D. Stojanovski, Mitochondrial protein transport in health and disease, Semin. Cell Dev. Biol. 76 (2018) 142–153.

[16] S.A. Paschen, U. Rothbauer, K. Káldi, M.F. Bauer, W. Neupert, M. Brunner, The role of the TIM8–13 complex in the import of Tim23 into mitochondria, EMBO J. 19 (2000) 6392–6400.

[17] D. Leuenberger, N.A. Bally, G. Schatz, C.M. Koehler, Different import pathways through the mitochondrial intermembrane space for inner membrane proteins, EMBO J. 18 (1999) 4816–4822.

[18] C.M. Koehler, E. Jarosch, K. Tokatlidis, K. Schmid, R.J. Schweyen, G. Schatz, Import of mitochondrial carriers mediated by essential proteins of the intermembrane space, Science 279 (1998) 369–373.

[19] K. Weinhäupl, C. Lindau, A. Hessel, Y. Wang, C. Schütze, T. Jores, L. Melchionda, B. Schönfisch, H. Kalbacher, B. Bersch, et al., Structural basis of membrane protein chaperoning through the mitochondrial intermembrane space, Cell 175 (2018) 1365–1379 (e25).

[20] C. Sirrenberg, M. Endres, H. Fölsch, R.A. Stuart, W. Neupert, M. Brunner, Carrier protein import into mitochondria mediated by the intermembrane proteins Tim10/Mrs11 and Tim12/Mrs5, Nature 391 (1998) 912–915.

[21] O. Kerscher, J. Holder, M. Srinivasan, R.S. Leung, R.E. Jensen, The Tim54p–Tim22p complex mediates insertion of proteins into the mitochondrial inner membrane, J. Cell Biol. 139 (1997) 1663–1675.

[22] Gebert, N., Gebert, M., Oeljeklaus, S., Malsburg, von der, K., Stroud, D.A., Kulawiak, B., Wirth, C., Zahedi, R.P., Dolezal, P., Wiese, S., et al. (2011). Dual function of Sdh3 in the respiratory chain and TIM22 protein translocase of the mitochondrial inner membrane. Mol. Cell 44, 811–818.

[23] C. Sirrenberg, M.F. Bauer, B. Guiard, W. Neupert, M. Brunner, Import of carrier proteins into the mitochondrial inner membrane mediated by Tim22, Nature 384 (1996) 582–585.

[24] O. Kerscher, N.B. Sepuri, R.E. Jensen, Tim18p is a new component of the Tim54p–Tim22p translocon in the mitochondrial inner membrane, Mol. Biol. Cell 11 (2000) 103–116.

[25] L. Ellenrieder, M.P. Dieterle, K.N. Doan, C.U. Mårtensson, A. Floerchinger, M.L. Campo, N. Pfanner, T. Becker, Dual role of mitochondrial porin in metabolite transport across the outer membrane and protein transfer to the inner membrane, Mol. Cell 73 (2019) 1056–1065.
[26] H. Sakaue, T. Shiota, N. Ishizaka, S. Kawano, Y. Tamura, K.S. Tan, K. Imai, C. Motono, T. Hirokawa, K. Taki, et al., Porin associates with Tom22 to regulate the mitochondrial protein gate assembly, Mol. Cell 73 (2019) 1044–1055.
[27] S. Callegari, F. Richter, K. Chojnacka, D.C. Jans, I. Lorenzi, D. Pacheu-Grau, S. Jakobs, C. Lenz, H. Urlaub, J. Dudek, et al., TIM29 is a subunit of the human carrier translocase required for protein transport, FEBS Lett. 590 (2016) 4147–4158.
[28] Y. Kang, M.J. Baker, M. Liem, J. Louber, M. McKenzie, I. Atukorala, C.-S. Ang, S. Keerthikumar, S. Mathivanan, D. Stojanovski, Tim29 is a novel subunit of the human TIM22 translocase and is involved in complex assembly and stability, Elife 5 (2016).
[29] M. Vukotic, H. Nolte, T. König, S. Saita, M. Ananjew, M. Krüger, T. Tatsuta, T. Langer, Acylglycerol kinase mutated in Sengers syndrome is a subunit of the TIM22 protein translocase in mitochondria, Mol. Cell 67 (2017) 471–483 (e477).
[30] Y. Kang, D.A. Stroud, M.J. Baker, D.P. De Souza, A.E. Frazier, M. Liem, D. Tull, S. Mathivanan, M.J. McConville, D.R. Thorburn, et al., Sengers syndrome-associated mitochondrial acylglycerol kinase is a subunit of the human TIM22 protein import complex, Mol. Cell 67 (2017) 457–470 (e5).
[31] A.K. Alkhaja, D.C. Jans, M. Nikolov, M. Vukotic, O. Lytovchenko, F. Ludewig, W. Schliebs, D. Riedel, H. Urlaub, S. Jakobs, et al., MINOS1 is a conserved component of mitofilin complexes and required for mitochondrial function and cristae organization, Mol. Biol. Cell 23 (2012) 247–257.
[32] V. Guarani, E.M. McNeill, J.A. Paulo, E.L. Huttlin, F. Fröhlich, S.P. Gygi, D. Van Vactor, J.W. Harper, QIL1 is a novel mitochondrial protein required for MICOS complex stability and cristae morphology, Elife 4 (2015).
[33] Malsburg, von der, K., Müller, J.M., Bohnert, M., Oeljeklaus, S., Kwiatkowska, P., Becker, T., Loniewska-Lwowska, A., Wiese, S., Rao, S., Milenkovic, D., et al. (2011). Dual role of mitofilin in mitochondrial membrane organization and protein biogenesis. Dev. Cell 21, 694–707.
[34] M. Harner, C. Körner, D. Walther, D. Mokranjac, J. Kaesmacher, U. Welsch, J. Griffith, M. Mann, F. Reggiori, W. Neupert, The mitochondrial contact site complex, a determinant of mitochondrial architecture, EMBO J. 30 (2011) 4356–4370.
[35] S. Hoppins, S.R. Collins, A. Cassidy-Stone, E. Hummel, R.M. Devay, L.L. Lackner, B. Westermann, M. Schuldiner, J.S. Weissman, J. Nunnari, A mitochondrial-focused genetic interaction map reveals a scaffold-like complex required for inner membrane organization in mitochondria, J. Cell Biol. 195 (2011) 323–340.
[36] C. Körner, M. Barrera, J. Dukanovic, K. Eydt, M. Harner, R. Rabl, F. Vogel, D. Rapaport, W. Neupert, A.S. Reichert, The C-terminal domain of Fcj1 is required for formation of crista junctions and interacts with the TOB/SAM complex in mitochondria, Mol. Biol. Cell 23 (2012) 2143–2155.
[37] M.A. Huynen, M. Mühlmeister, K. Gotthardt, S. Guerrero-Castillo, U. Brandt, Evolution and structural organization of the mitochondrial contact site (MICOS) complex and the mitochondrial intermembrane space bridging (MIB) complex, Biochim. Biophys. Acta 1863 (2016) 91–101.
[38] M. Barbot, D.C. Jans, C. Schulz, N. Denkert, B. Kroppen, M. Hoppert, S. Jakobs, M. Meinecke, Mic10 oligomerizes to bend mitochondrial inner membranes at cristae junctions, Cell Metab. 21 (2015) 756–763.
[39] M. Bohnert, R.M. Zerbes, K.M. Davies, A.W. Mühleip, H. Rampelt, S.E. Horvath, T. Boenke, A. Kram, I. Perschil, M. Veenhuis, et al., Central role of Mic10 in the mitochondrial contact site and cristae organizing system, Cell Metab. 21 (2015) 747–755.
[40] D. Tarasenko, M. Barbot, D.C. Jans, B. Kroppen, B. Sadowski, G. Heim, W. Möbius, S. Jakobs, M. Meinecke, The MICOS component Mic60 displays a conserved membrane-bending activity that is necessary for normal cristae morphology, J. Cell Biol. 216 (2017) 889–899.
[41] M. Hessenberger, R.M. Zerbes, H. Rampelt, S. Kunz, A.H. Xavier, B. Purfürst, H. Lilie, N. Pfanner, M. van der Laan, O. Daumke, Regulated membrane remodeling by Mic60 controls formation of mitochondrial crista junctions, Nat. Commun. 8 (2017), 15258.
[42] Bohnert, M., Wenz, L.-S., Zerbes, R.M., Horvath, S.E., Stroud, D.A., Malsburg, von der, K., Müller, J.M., Oeljeklaus, S., Perschil, I., Warscheid, B., et al. (2012). Role of mitochondrial inner membrane organizing system in protein biogenesis of the mitochondrial outer membrane. Mol. Biol. Cell 23, 3948–3956.
[43] R. Anand, V. Strecker, J. Urbach, I. Wittig, A.S. Reichert, Mic13 is essential for formation of crista junctions in mammalian cells, PLoS One 11 (2016), e0160258.
[44] S. Schorr, M. van der Laan, Integrative functions of the mitochondrial contact site and cristae organizing system, Semin. Cell Dev. Biol. 76 (2018) 191–200.
[45] C. Ding, Z. Wu, L. Huang, Y. Wang, J. Xue, S. Chen, Z. Deng, L. Wang, Z. Song, S. Chen, Mitofilin and CHCHD6 physically interact with Sam50 to sustain cristae structure, Sci. Rep. 5 (2015), 16064.
[46] D.I. Kim, S.C. Jensen, K.A. Noble, B. Kc, K.H. Roux, K. Motamedchaboki, K.J. Roux, An improved smaller biotin ligase for BioID proximity labeling, Mol. Biol. Cell 27 (2016) 1188–1196.
[47] M. Ashburner, C.A. Ball, J.A. Blake, D. Botstein, H. Butler, J.M. Cherry, A.P. Davis, K. Dolinski, S.S. Dwight, J.T. Eppig, et al., Gene ontology: tool for the unification of biology. The Gene Ontology Consortium, Nat. Genet. 25 (2000) 25–29.
[48] C. Glytsou, E. Calvo, S. Cogliati, A. Mehrotra, I. Anastasia, G. Rigoni, A. Raimondi, N. Shintani, M. Loureiro, J. Vazquez, et al., Optic atrophy 1 is epistatic to the core MICOS component MIC60 in mitochondrial cristae shape control, Cell Rep. 17 (2016) 3024–3034.
[49] P. Rehling, K. Model, K. Brandner, P. Kovermann, A. Sickmann, H.E. Meyer, W. Kühlbrandt, R. Wagner, K.N. Truscott, N. Pfanner, Protein insertion into the mitochondrial inner membrane by a twin-pore translocase, Science 299 (2003) 1747–1751.
[50] E.J. De Genst, T. Guilliams, J. Wellens, E.M. O'Day, C.A. Waudby, S. Meehan, M. Dumoulin, S.-T.D. Hsu, N. Cremades, K.H.G. Verschueren, et al., Structure and properties of a complex of α-synuclein and a single-domain camelid antibody, J. Mol. Biol. 402 (2010) 326–343.
[51] K. Wagner, N. Gebert, B. Guiard, K. Brandner, K.N. Truscott, N. Wiedemann, N. Pfanner, P. Rehling, The assembly pathway of the mitochondrial carrier translocase involves four preprotein translocases, Mol. Cell. Biol. 28 (2008) 4251–4260.
[52] P. Paumard, J. Vaillier, B. Coulary, J. Schaeffer, V. Soubannier, D.M. Mueller, D. Brèthes, J.-P. di Rago, J. Velours, The ATP

synthase is involved in generating mitochondrial cristae morphology, EMBO J. 21 (2002) 221–230.
[53] K.M. Davies, C. Anselmi, I. Wittig, J.D. Faraldo-Gómez, W. Kühlbrandt, Structure of the yeast F1Fo-ATP synthase dimer and its role in shaping the mitochondrial cristae, Proc. Natl. Acad. Sci. U. S. A. 109 (2012) 13602–13607.
[54] A. Hahn, K. Parey, M. Bublitz, D.J. Mills, V. Zickermann, J. Vonck, W. Kühlbrandt, T. Meier, Structure of a complete ATP synthase dimer reveals the molecular basis of inner mitochondrial membrane morphology, Mol. Cell 63 (2016) 445–456.
[55] H. Li, Y. Ruan, K. Zhang, F. Jian, C. Hu, L. Miao, L. Gong, L. Sun, X. Zhang, S. Chen, et al., Mic60/Mitofilin determines MICOS assembly essential for mitochondrial dynamics and mtDNA nucleoid organization, Cell Death Differ. 23 (2016) 380–392.
[56] C. Ott, K. Ross, S. Straub, B. Thiede, M. Götz, C. Goosmann, M. Krischke, M.J. Mueller, G. Krohne, T. Rudel, et al., Sam50 functions in mitochondrial intermembrane space bridging and biogenesis of respiratory complexes, Mol. Cell. Biol. 32 (2012) 1173–1188.
[57] J. Xie, M.F. Marusich, P. Souda, J. Whitelegge, R.A. Capaldi, The mitochondrial inner membrane protein mitofilin exists as a complex with SAM50, metaxins 1 and 2, coiled-coil-helix coiled-coil-helix domain-containing protein 3 and 6 and DnaJC11, FEBS Lett 581 (2007) 3545–3549.
[58] Zerbes, R.M., Bohnert, M., Stroud, D.A., Malsburg, von der, K., Kram, A., Oeljeklaus, S., Warscheid, B., Becker, T., Wiedemann, N., Veenhuis, M., et al. (2012). Role of MINOS in mitochondrial membrane architecture: cristae morphology and outer membrane interactions differentially depend on mitofilin domains. J. Mol. Biol. 422, 183–191.
[59] N. Mühlenbein, S. Hofmann, U. Rothbauer, M.F. Bauer, Organization and function of the small Tim complexes acting along the import pathway of metabolite carriers into mammalian mitochondria, J. Biol. Chem. 279 (2004) 13540–13546.
[60] N. Pfanner, B. Warscheid, N. Wiedemann, Mitochondrial proteins: from biogenesis to functional networks, Nat. Rev. Mol. Cell Biol. 20 (2019) 267–284.
[61] D. Pacheu-Grau, S. Callegari, S. Emperador, K. Thompson, A. Aich, S.E. Topol, E.G. Spencer, R. McFarland, E. Ruiz-Pesini, A. Torkamani, et al., Mutations of the mitochondrial carrier translocase channel subunit TIM22 cause early-onset mitochondrial myopathy, Hum. Mol. Genet. 27 (2018) 4135–4144.
[62] K. Roesch, S.P. Curran, L. Tranebjaerg, C.M. Koehler, Human deafness dystonia syndrome is caused by a defect in assembly of the DDP1/TIMM8a–TIMM13 complex, Hum. Mol. Genet. 11 (2002) 477–486.
[63] R.S. Sikorski, P. Hieter, A system of shuttle vectors and yeast host strains designed for efficient manipulation of DNA in *Saccharomyces cerevisiae*, Genetics 122 (1989) 19–27.
[64] M. Knop, K. Siegers, G. Pereira, W. Zachariae, B. Winsor, K. Nasmyth, E. Schiebel, Epitope tagging of yeast genes using a PCR-based strategy: more tags and improved practical routines, Yeast 15 (1999) 963–972.
[65] C. Janke, M.M. Magiera, N. Rathfelder, C. Taxis, S. Reber, H. Maekawa, A. Moreno-Borchart, G. Doenges, E. Schwob, E. Schiebel, et al., A versatile toolbox for PCR-based tagging of yeast genes: new fluorescent proteins, more markers and promoter substitution cassettes, Yeast 21 (2004) 947–962.
[66] C. Meisinger, N. Pfanner, K.N. Truscott, Isolation of yeast mitochondria, Methods Mol. Biol. 313 (2006) 33–39.
[67] F. Richter, S. Dennerlein, M. Nikolov, D.C. Jans, N. Naumenko, A. Aich, T. MacVicar, A. Linden, S. Jakobs, H. Urlaub, et al., ROMO1 is a constituent of the human presequence translocase required for YME1L protease import, J. Cell Biol. 218 (2019) 598–614.
[68] I. Wittig, H.-P. Braun, H. Schägger, Blue native PAGE, Nat. Protoc. 1 (2006) 418–428.
[69] I. Atanassov, H. Urlaub, Increased proteome coverage by combining PAGE and peptide isoelectric focusing: comparative study of gel-based separation approaches, Proteomics 13 (2013) 2947–2955.